PRINT ISSN 1119-8362
Electronic ISSN 2659-1499

Full-text Available Online at
https://www.ajol.info/index.php/jasem
https://www.bioline.org.br/ja

J. Appl. Sci. Environ. Manage.
Vol. 28 (9) 2641-2648 September 2024

Use of Tungsten Inert Gas Welding on Mild Steel Weldment to Optimize Welding Process Variables on Electrode Melting Rate

***OSADIAYE, NH; ACHEBO, JI**

Department of Production Engineering, University of Benin, Benin City, Nigeria

**Corresponding Author Email: nosayaba.osadiaye@uniben.edu*
**ORCID: https://orcid.org/0009-0000-7480-5520*
**Tel: +2348037441643*

Co-Author Email: josephachebo@yahoo.co.uk

ABSTRACT: One of the most crucial factors taken into account when evaluating the performance of Tungsten Inert Gas (TIG) welding is the Electrode Melting Rate, which shows how much of the heat deposited by the welding operation is used to generate melting. A dense weld pool forms in the field of welding when there is a good melting rate. Therefore, this paper investigates the use of tungsten inert gas welding on mild steel weldment to optimize welding process variables on electrode melting rate employing Artificial Neural Networks and Response Surface Methodology in the analysis. The ideal electrode melting rate of 4.6539 mm/s can be achieved by combining the following parameters: wire diameter of 2.55 mm, welding speed of 3.02 mm/s, and welding current of 208.22A, according to the RSM results. R values of 0.9119 were displayed by the RSM for the electrode melting rate. A regression plot of the ANN results indicates that the total R value is 0.93807. Because the Artificial Neural Network's output fits the experimental data more closely than the Response Surface Methodology's, it is chosen as the superior predictive model.

DOI: https://dx.doi.org/10.4314/jasem.v28i9.6

Cite this Article as: OSADIAYE, N. H; ACHEBO, J. I. (2024). Use of Tungsten Inert Gas Welding on Mild Steel Weldment to Optimize Welding Process Variables on Electrode Melting Rate. *J. Appl. Sci. Environ. Manage.* 28 (9) 2641-2648

Dates: Received: 04 July 2024; Revised: 08 August 2024; Accepted: 12 August July 2024 Published: 05 September 2024

Keywords: Electrode melting rate; Weldment; tungsten inert gas welding; mild steel welds; r0esponse surface methodology; artificial neural network

Welding with tungsten inert gas (TIG), renowned for its precision and versatility, is a favored welding technique in industries where high-quality welds are imperative (Chaturvedi and Vendan, 2022). One of these critical intricacies is the electrode melting rate, a parameter that often operates behind the scenes but wields substantial influence over the welding process. In this research, we delve into the significance of electrode melting rate in TIG welding, the factors that govern it, its measurement, control, and its profound implications for welding quality and efficiency. Achieving deep penetration in TIG welding is pivotal, particularly when joining thick materials (Pavan *et al*., 2021). The importance of electrode melting rate in TIG welding cannot be overstated. It directly affects the amount of filler material delivered to the weld pool, influencing weld penetration and overall quality (Wu and Krivtsun, 2020). Deep penetration is essential for guaranteeing the weld's structural integrity and the reliability of the joint (Schmoeller *et al*., 2022). Optimizing electrode melting rate is the key to achieving deep penetration while maintaining weld quality (Mvola *et al*., 2018). This optimization process involves meticulous adjustment of welding

**Corresponding Author Email: nosayaba.osadiaye@uniben.edu*
**ORCID: https://orcid.org/0009-0000-7480-5520*
**Tel: +2348037441643*

parameters, thoughtful selection of electrode material and geometry, and appropriate shielding gas management (Aldalur *et al.,* 2023). The importance of electrode melting rate in TIG welding cannot be understated. It is a fundamental aspect that dictates the rate at which the tungsten electrode, an essential component of the TIG welding torch, melts during the welding process (Shravan *et al*., 2023). This melting process directly affects the stability of the arc, the transfer of filler material into the welding area, and, ultimately, the quality of the resulting weld (Yang *et al*., 2020). Several factors contribute to the modulation of electrode melting rate. Foremost among these is the control over welding variables. Variables such as arc voltage, welding current, and speed of travel directly influence the electrode's heating and melting characteristics (Zhang *et al.*, 2023). Meticulous adjustment of these parameters allows welders to attain the desired electrode melting rate for a particular welding application. The choice of electrode material, its purity, and its diameter play pivotal roles in determining electrode melting rate. Different electrode materials exhibit varying melting points and conductivity, impacting the rate at which the electrode melts (Lekshmi *et al*., 2023). Additionally, the geometry of the electrode tip, such as its shape and size, affects the melting process and the characteristics along the arc. The choice and flow rate of the shielding gas enveloping the welding arc significantly affect the arc's stability and, consequently, the electrode's melting rate. Shielding gas control is vital for maintaining an optimal environment for controlled electrode melting (Astafeva and Astafev, 2018). Accurate measurement of electrode melting rate is paramount for TIG welding quality monitoring and process management. Various methods are employed for this purpose, including direct observation, high-speed imaging, and monitoring the length of the electrode consumed during welding (Cho *et al*., 2022). These techniques provide valuable insights into the melting rate and allow welders to adjust their approach as needed. Control over electrode melting rate is a hallmark of a skilled TIG welder. It requires a deep understanding of welding parameters and electrode characteristics. The ability to fine-tune welding parameters to achieve the desired melting rate is essential for producing consistent and high-quality welds. The implications of electrode melting rate reach far beyond the technical aspects of welding. Precision is the essence of TIG welding, and the controlled melting of the tungsten electrode is the key to achieving this precision. It directly influences the stability of the arc, the transfer of filler material, and the resulting weld quality. A controlled melting rate ensures a stable and focused arc, which is critical for intricate and high-precision welding applications, such as aerospace and medical device manufacturing (He & Xing, 2019). Efficiency is another critical dimension influenced by electrode melting rate. An optimized melting rate not only ensures precise welds but also contributes to the efficiency of the welding process. Higher efficiency translates to increased productivity and cost savings in various welding operations. Experimental studies play a pivotal role in validating predictive models and optimizing electrode melting rates. Researchers conduct experiments to measure actual melting rates, assess weld quality, and evaluate the mechanical properties of the welded joint under varying welding conditions (Chinnadurai *et al*., 2021). Empirical data serve as the foundation for the validation and refinement of predictive models (Wang *et al.*, 2018). Electrode melting rate in TIG welding is a subtle yet crucial component of precision welding. It is a parameter that, when harnessed with expertise, allows TIG welders to create consistent, high-quality welds. Control over electrode melting rate is a testament to the skill and craftsmanship required in the world of TIG welding, where the controlled melting of the tungsten electrode ultimately shapes the precision and quality of the final product. In this study, advanced predictive models was applied to dynamically optimize electrode melting rates during TIG welding. Additionally, exploring innovative electrode materials and shielding gas compositions holds promise for further elevating weld quality and efficiency. Collaborative efforts and the integration of Industry 4.0 concepts will be instrumental in driving innovation in this critical area of welding technology. Therefore, the objective of this paper as to investigates the use of tungsten inert gas welding on mild steel weldment to optimize welding process variables on electrode melting rate employing Artificial Neural Networks and Response Surface Methodology

MATERIALS AND METHODS

One of the most effective welding techniques employed in this study is the gas tungsten arc welding method to join the test coupons. The mild steel dish is cleaned and bevelled before the welding process. To shield the weld specimen from acclimate interaction when welds are being created, pure argon gas was employed. Mild steel plates were used as weld samples in which the joints were carefully welded, and the resulting measurements meticulously recorded. Twenty different sets of experiments were conducted for this research. To enable the connecting of two mild steel plates of 60 x 40 x 10mm, welding current, welding rate, and wire diameter were adjusted throughout each trial run.

Response Surface Methodology (RSM): Engineers seeking the circumstances that will accelerate their

target process would go for Response Surface Methodology (RSM). Response Surface Methodology (RSM) is an extensively employed improvement technique for assessing welding process performance and determining the optimal values for desired responses. RSM includes a group of statistical and theoretical tools that are effective in designing and forecasting reactions affected by a variety of input factors, all having the overarching goal of optimizing these responses. The optimization of the response surface methodology relies on a second-order polynomial equation, which is provided as a response algorithm within user-friendly statistical software. This facilitates straightforward comparisons of the performance of various approximating functions of different orders.

Artificial Neural Network (ANN): Neural networks serve as invaluable data mining tools for uncovering concealed patterns within databases. These networks operate as widely distributed, massively parallel processors with a built-in capability for assimilating experiential learning and accessibility for various applications. In two key aspects, they share a resemblance with the human brain in the sense that the acquisition of knowledge occurs through learning, and this knowledge is kept in using strength of interneuron connections referred to as synaptic weights.

RESULTS AND DISCUSSION

Modeling and Optimization using Response Surface Methodology (RSM): To substantiate the appropriateness in the context of the quadratic model used for examining the test results, sum of squares for the sequential model in the electrode melting rate was calculated, as shown in Table 1. To assess the capacity of the quadratic formulation in elucidating the inherent variation linked to the experimental data, and the inability to fit test was conducted each response, individually. A model exhibiting a pronounced fit insufficience is not suitable for making predictions. The outcomes of the calculated fit lack test for droplet velocity are detailed in Table 2. Considering the results of Table 3, it was also discovered that the cubic polynomial showed a substantial lack of fit and was therefore excluded from the analysis of the model, but the quadratic polynomial demonstrated a modest but not significant lack of fit. The statistics pertaining to the droplet velocity response, derived from the model sources, are presented in Table 3.

Table 1: Sum of squares for the sequential model of Electrode melting rate

Origin	Sum of Squares	df	Mean Square	F Value	p-value Prob. > F	
Mean vs Total	432.93	1	432.93			
Linear vs Mean	1.14	3	0.38	0.34	0.7973	
2FI vs Linear	3.53	3	1.18	1.07	0.3962	
Quadratic vs 2FI	12.66	3	4.22	25.19	< 0.0001	Suggested
Cubic vs Quadratic	0.13	4	0.033	0.13	0.9672	Aliased
Residual	1.54	6	0.26			
Total	570.43	20	22.60			

Table 2: Droplet velocity lack of fit test

Origin	Sum of Squares	Df	Avg Square	F Value	p-value Prob.> F	
Linear	8.46	11	0.77	5.70	0.0337	
2FI	7.23	8	0.90	6.70	0.0255	
Quadratic	0.28	5	0.057	0.42	0.8170	Suggested
Cubic	0.16	1	0.16	1.15	0.3316	Aliased
Pure Error	0.67	5	0.13			

Table 3: Summary stats for the model droplet velocity

Origin	**Std. Dev.**	**R-Squared**	**Adjusted R-Squared**	**Predicted R-Squared**	**PRESS**	
Linear	0.76	0.3121	0.1833	-0.0445	13.88	
2FI	0.78	0.4053	0.1308	-0.1375	15.11	
Quadratic	0.31	0.9278	0.8628	0.7600	3.19	Suggested
Cubic	0.51	0.9375	0.8021	-1.6578	35.31	Aliased

The model fit statistics in brief include the standard deviation, R- squared, adjusted R-squared, anticipated R- squared, and predicted error sum of squares (PRESS) statistic for every comprehensive model. The ideal standards for determining the top source for models are a minimal standard deviation an R- squared value close to 1, and PRESS is comparatively low. Considering the outcomes presented in Table 4, the algorithm for quadratic polynomials was recommended, as opposed to the cubic polynomial

model, omitted. Consequently, this analysis used the quadratic polynomial model. An ANOVA was performed to determine the algorithm's importance, and to assess the individual contributions of each variable, as well as the quadratic and cumulative impacts on every response. the Model F-value had 11.50 which indicates that the algorithm is indeed important. Only 0.13% of the time is there a probability that such a big "Model F-Value" possibly because of unpredictable noise. Model terms with "Prob > F" values < 0.0500 are considered significant. In this case, variables A, B, C, A B, A C, A^2, B^2, and C^2 are all essential model terms. Higher values of 0.1000 suggest that the model terms don't matter. The "Lack of Fit F-value" of 1.08 suggests that when weighed against pure inaccuracy, the Lack of Fit is not substantial. A "Lack of Fit F-value" this large could be, 98.78% of the time noise is to blame. An insignificant mismatch is positive, as it indicates the significance of the algorithm. To verify the effectiveness of the quadratic model in reducing the electrode melting rate, the GOF statistics can be found in Table 4. Based on the results presented in Table 5, it is evident that "Predicted R-Squared" value of 0.8332 closely aligns with the "Adj R-Squared" value of 0.8325. The adequate precision, which checks the signal-to-noise ratio, is a key indicator. A ratio larger than 4 is deemed acceptable. In this case, the computed ratio of 10.553, as observed in Table 5, indicates a highly adequate signal. This suggests that the algorithm is dependable and could be effectively utilized to explore the creative area and efficiently minimize the electrode melting rate. To assess model of the response surface's statistical properties, electrode melting rate normal probability plot with studentized residuals is displayed in Figure1. It can be observed that the points on the plot generally follow a straight line, despite some slight scatter. There is no discernible pattern such as an S-shaped curve apart from the linear trend. This suggests that the residuals exhibit a normal distribution, and there is no need for data transformation to enhance the analysis. Additionally, the studentized residuals' normal probability plot was utilized to evaluate the estimated residuals' normality. This plot, which represents the amount of standardized deviations of real values relative to expected values, was used to verify whether the (observed - anticipated) residuals adhere to a regular circulation. This assessment is crucial for evaluating the adequacy of an analytical framework. The outcomes in Figure 1 indicate that the computed residuals exhibit an approximate normal distribution, affirming that the developed model is satisfactory.

To detect for the existence of mega patterns or expanding variance a plot of residuals and the predicted was produced for Electrode melting rate that is depicted in Figure 2.

Table 4: GOF statistics for minimizing Electrode melting rate

Std. Dev.	0.41	R – Squared	0.9119
Avg	4.65	Adj R – Squared	0.8325
C.V. %	8.80	Pred R - Squared	0.8332
P.R.E.S.S	3.36	Adeq Precision	10.553

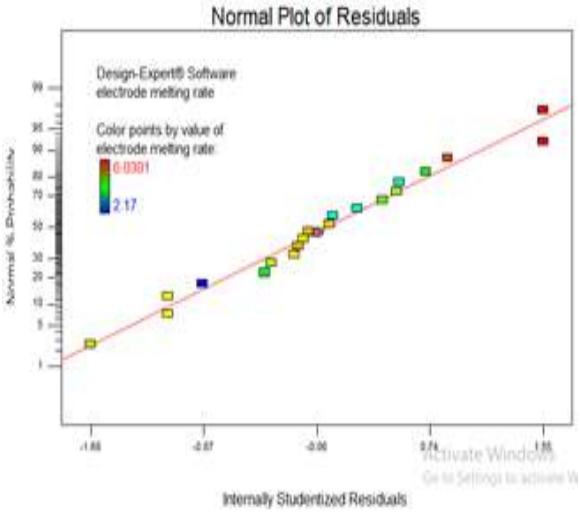

Fig 1: Electrode melting rate normal probability plot with studentized residuals

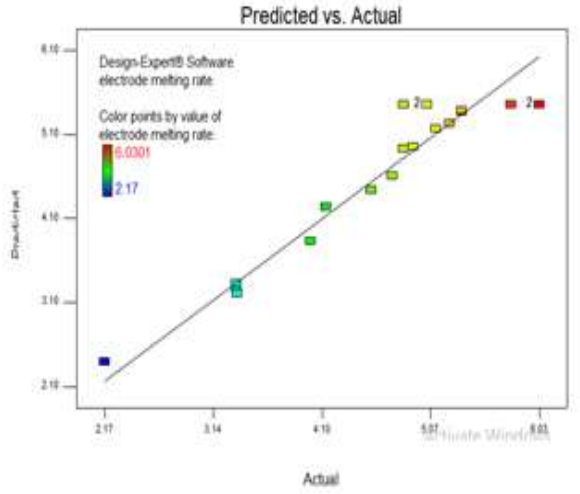

Fig 2: Plot of Residual vs. Predicted electrode melting rate

As evident the graph shows, the data dots are closely aligned with the fit line. The algorithm demonstrates its ability to effectively forecast the majority of the data dots. To identify potential outliers results from the experiment show a Cook's distance plot was created for various outcomes. Cook's distance serves as a measurement of the regression's magnitude results would alter if a particular point (observation) were excluded, the evaluation revealed. A dot with a

significantly high Cook's distance compared to the rest, it can be unusual and warrants further investigation. The electrode melting rate's Cook's distance plot is illustrated in Figure 3.

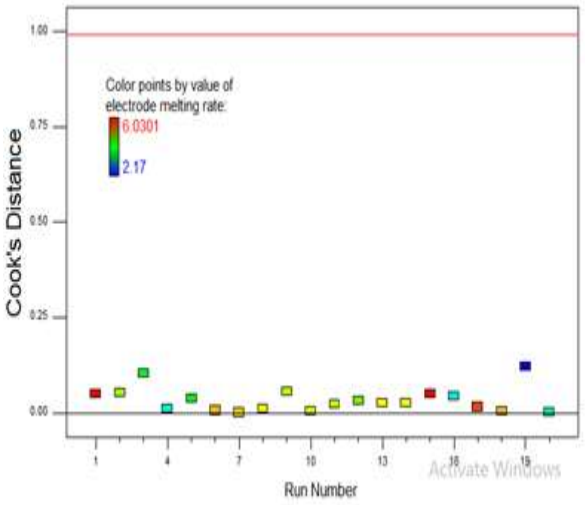

Fig 3: Cook's distance for Electrode melting rate

The maximum and bottom limits of the Cook's distance plot are 1.00 and 0.00, respectively. Test results falling below lower limit, or exceeding the upper bound are typically regarded as anomalies and should be subject to a thorough investigation. The results in Figure 3 indicate that the data used in this analysis do not contain any apparent outliers, affirming the reliability results of the trial. To explore the impacts of welding current and the welding rate on the electrode melting rate, 3-D surface plots were generated, as depicted in Figure 4, using the following procedure:

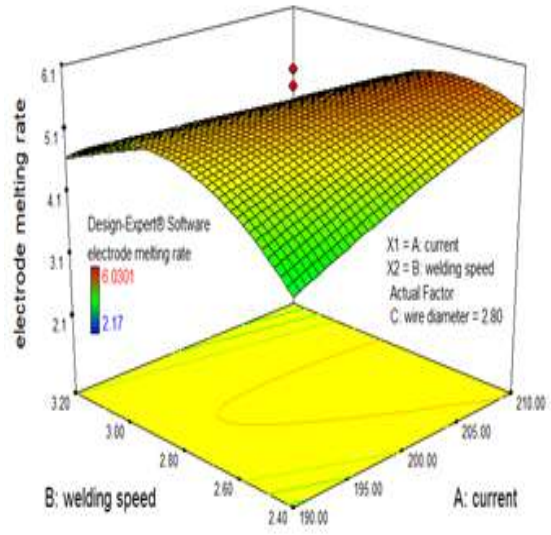

Fig 4: 3D Plot of Welding Current and Welding Speed on Electrode Melting Rate

Using 3-D surface plots, researchers may examine how welding current and wire diameter affect the electrode melting rate, as shown in Figure 5, were created through the following process:

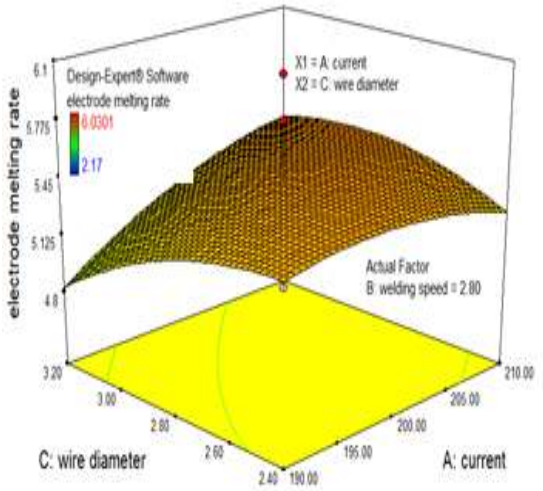

Fig 5: 3D Plot of Welding Current and Wire Diameter on Electrode Melting Rate

Using 3D surface plots, researchers may examine how welding speed and wire diameter affect the electrode melting rate, as displayed in Figure 6, were created using the following procedure:

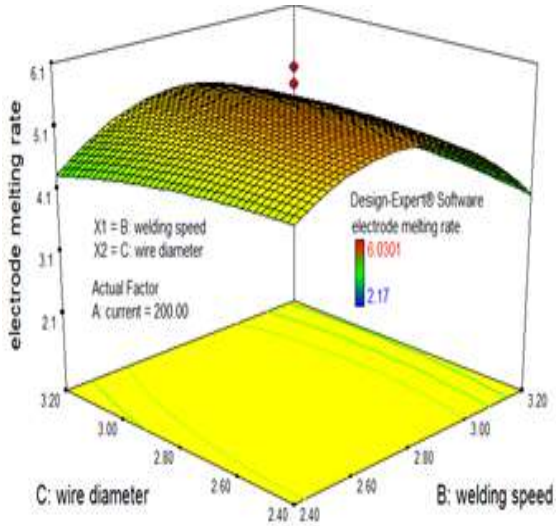

Fig 6: 3D Plot of wire diameter and welding speed on the rate of melting of the electrode

The 3-D surface plot, as depicted in Figure 6, illustrates the connection involving the input parameters (welding current, welding speed, and wire diameter) and the reaction parameter (Electrode melting rate). This plot provides a three-dimensional visualization to offer a vivid understanding within the

reaction surface. While not as effective as contour plots for determining locations and reaction values, it can provide a more intuitive depiction about the top. In this plot, as the color of the curved top becomes darker, it signifies a proportional decrease in the electrode melting rate. When there is a colored depression in the center of the upper surface suggests that some points, for simpler recognition, it is faintly tinted, are located underneath the surface. Upon examination of the surface plot in Figure 6, it becomes apparent that the color of the surface gets lighter towards the current and also the welding speed. The implication is that an increase in current and welding speed will lead to a proportionate increase in Electrode melting rate. Numerical optimization was implemented to determine the desirability of the overall model. In the numerical optimization phase, design expert was used minimize the electrode melting rate response as shown in Table 5.

Table 5: Numerical optimal solutions

Number	Current	Welding speed	Wire diameter	Electrode melting	Desirability	
1	**208.22**	**3.02**	**2.55**	**4.6539**	**0.673**	**Selected**
2	210.00	244	2.88	5.46051	0.666	
3	210.00	241	2.87	5.4096	0.665	

Modeling and prediction utilizing an artificial neural network (ANN): Neural networks are composed of interconnected nodes, and the specific types of connections and patterns of connectivity among these nodes can vary. However, the most common type of connection is the layered connection; the squared nodes boxes are used to represent the input nodes. Input nodes, also known as input neurons, serve the role of transmitting input signals. They do not perform any calculations, such as the weighted sum, and they do not apply any activation functions. Output nodes, on the other hand, produce the final output of the neural network. The middle nodes in a neural network, hidden layers are those that exist between the input and output layers. They are labeled 'hidden' given that they cannot be reached via the exterior of the neural network and do not directly interact with the input or output. Over time, neural networks have evolved from a simple architecture to more complex configurations, known as deep neural networks. The input matrix contains current, weld speed and wire diameter, making it a 3x20 matrix since 20 runs were conducted. Figure 7 depicts the Network attributes interphase for predicting weld electrode melting rate response, hence, the feedforward backpropagation method was selected among other network types to achieve the most favorable results.

Figure 8 shows the performance curve for the trained network, indicating that the best validation performance was achieved at epoch 4 while Figure 9 shows the neural network gradient plot for predicting electrode melting rate responses.

In the MATLAB software, an epoch represents a complete iteration of the training process for the neural network. This means that once all the data vectors in your training set have been processed through your training algorithm, one epoch has been completed. The actual time duration of an epoch can vary depending on the training method employed. In this case, the optimal prediction for the transverse responses was achieved at epoch 4, even though a total of 6 epochs were used in the iteration process. This suggests that the model's performance had stabilized and further iterations did not significantly improve the results.

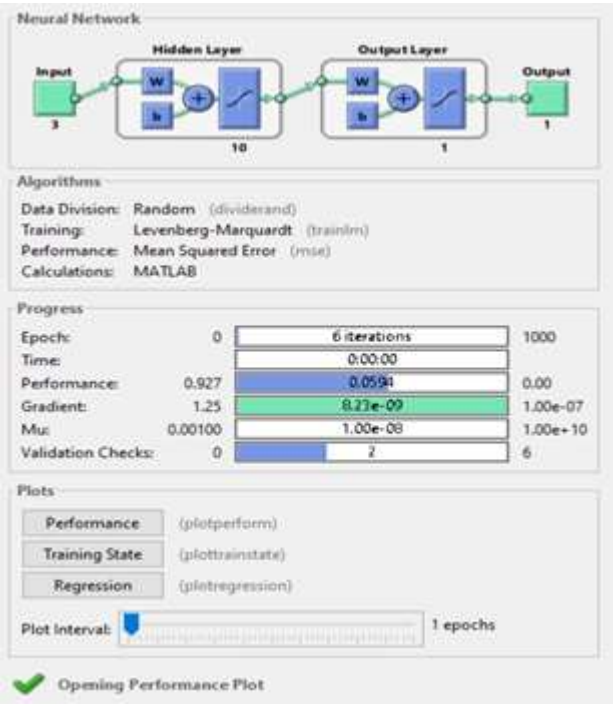

Fig 7: Network attributes interphase for predicting weld electrode melting rate response

Figure 8 illustrates how many epochs there are used during the training process. Each epoch stands for one complete training iteration of the algorithm.

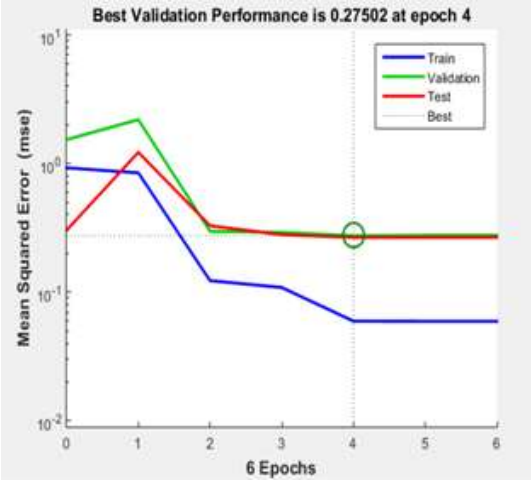

Fig 8: Performance curve using a trained network

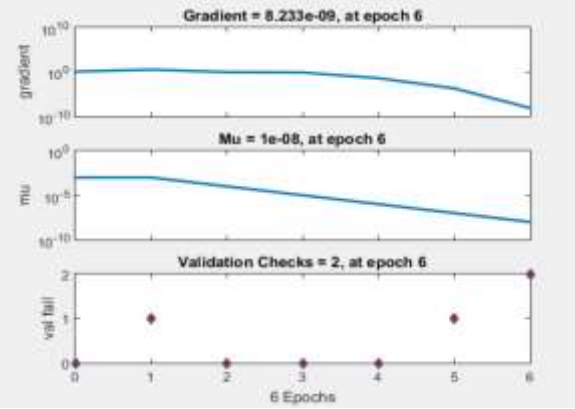

Fig 9: Neural network gradient plot

In this case, a total of 6 epochs were used, and it's apparent from the chart the most accurate forecast was obtained at the 4th epoch. The dotted red lines in Figure 9, used for validation checks, clearly indicate that the lowest error occurred at epoch 4, reinforcing the idea that the model's performance was optimized at that point. Figure 10 displays the instruction, testing, and validation plots with a correlation coefficient (R) exceeding 70%. This indicates a robust prediction for the Fume Formation Rate. Each plot's dotted diagonal line represents the best-fit line, and a correlation of 1 along this line would signify a perfect prediction. While the correlation coefficient may not reach 1 in this case, a value above 70% suggests a strong and reliable predictive relationship for the Fume Formation Rate.

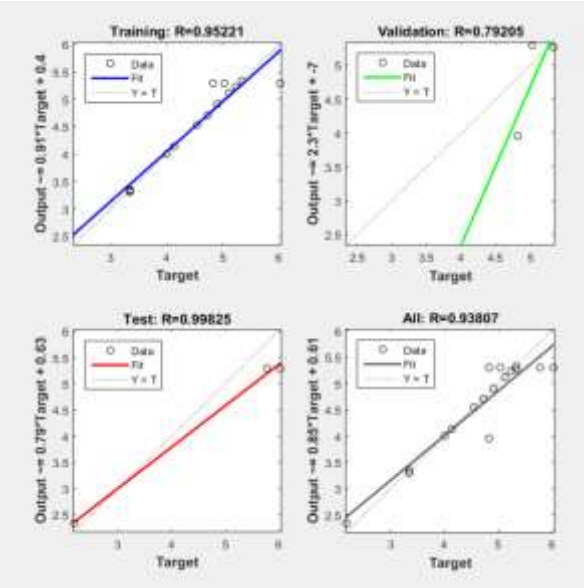

Fig 10: Training, validation, and testing for electrode melting rate responses in a regression plot

Table 6: **Experimental electrode melting vs ANN prediction**.

	Current	weld	wire	Exp	ANN	Prediction Error
1	200.00	2.80	2.80	6.0301	5.29436682422187	0.735733175778132
2	190.00	3.20	2.40	4.7224	4.71155009163901	0.0108499083609956
3	210.00	3.20	3.20	4.0000	3.99599540005464	0.00400459994536195
4	210.00	3.20	2.40	3.3370	3.30159876089171	0.0354012391082867
5	190.00	2.40	2.40	4.1330	4.13231186678608	0.000688133213917475
6	216.82	2.80	2.80	5.3370	5.26393567532366	0.0730643246763387
7	200.00	2.80	2.13	5.2342	5.22961788746490	0.00458211253510044
8	210.00	2.40	3.20	5.1116	5.11148703211439	0.000112967885611326
9	200.00	2.80	2.80	4.8241	5.29436682422187	-0.470266824221868
10	183.18	2.80	2.80	4.9081	4.90780845263214	0.000291547367864631
11	200.00	2.80	3.47	4.8241	3.95814340360403	0.865956596395972
12	190.00	3.20	3.20	4.5379	4.53696310306167	0.000936896938331877
13	200.00	2.80	2.80	5.0301	5.29436682422187	-0.264266824221868
14	200.00	2.80	2.80	5.0301	5.29436682422187	-0.264266824221868
15	200.00	2.80	2.80	6.0301	5.29436682422187	0.735733175778132
16	200.00	2.13	2.80	3.3420	3.34196254955168	3.74504483180438e-05
17	200.00	2.80	2.80	5.7751	5.29436682422187	0.480733175778132
18	210.00	2.40	2.40	5.3370	5.33562895983747	0.00137104016253353
19	200.00	3.47	2.80	2.1700	2.33852999882220	-0.168529998822198
20	190.00	2.40	3.20	3.3378	3.33778157326300	1.84267369998103e-05

Conclusion: A close examination of the molten metal transfer rate and droplet diameter required for deep penetration during globular to spray was experimented with three (3) process parameters namely: welding current, welding speed and wire diameter to predict and to optimize the MMTR and droplet diameter required for deep penetration with electrode melting rate using RSM and ANN. Welding current and welding speed are the parameters having the most significant effect on deep penetration and transfer modes .The results from this study shows that ANN is a better predictive tool than RSM

REFERENCES

Aldalur, E; Suárez, A; Curiel, D; Veiga, F; Villanueva, P (2023). Intelligent and Adaptive System for Welding Process Automation in T-Shaped Joints. *Metals*, *13*(9): 1532.

Astafeva, N; Astafev, A (2018). Analysis of erosion susceptibility for tungsten electrodes in submerged arc welding. *Inter. Confer. Aviamech. Engineer. Transport. (AVENT* .30-34. Atlantis Press.

Chaturvedi, M; Vendan, S. A (2022). Advanced Welding Techniques. Springer Verlag, Singapore.

Chinnadurai, T; Prabaharan, N; Saravanan, S; Pandean, M. K; Pandiyan, P; Alhelou, H. H (2021). Prediction of process parameters of ultrasonically welded PC/ABS material using soft-computing techniques. *IEEE Access*, *9*: 33849-33859.

Cho, H. W; Shin, S. J; Seo, G. J; Kim, D. B; Lee, D. H (2022). Real-time anomaly detection using convolutional neural network in wire arc additive manufacturing: molybdenum material. *J. Mater. Process. Technol*, *302*: 117495.

He, Y; Xing, Z (2019). Investigations on the microstructure, mechanical properties and corrosion resistance of SUS 304 austenitic stainless steel welded joints by pulsed current gas tungsten arc welding. *Mater. Reseach.Expr*, *6*(8): 088001.

Lekshmi, G. S; Bazaka, K; Ramakrishna, S; Kumaravel, V (2023). Microbial electrosynthesis: carbonaceous electrode materials for CO_2 conversion. *Mater. Horizons*, *10*(2): 292-312.

Mvola, B; Kah, P; Layus, P (2018). Review of current waveform control effects on weld geometry in gas metal arc welding process. *The Inter. J. Adv. Manu. Technol. 96*: 4243-4265.

Pavan, A. R; Chandrasekar, N; Arivazhagan, B; Kumar, S; Vasudevan, M (2021). Study of arc characteristics using varying shielding gas and optimization of activated-tig welding technique for thick AISI 316L (N) plates. *CIRP J. Manu. Sci. Techno. 35*: 675-690.

Schmoeller, M; Weiss, T; Goetz, K; Stadter, C; Bernauer, C; Zaeh, M. F (2022). Inline Weld Depth Evaluation and Control Based on OCT Keyhole Depth Measurement and Fuzzy Control. *Processes. 10*(7): 1422.

Shravan, C; Radhika, N; Kumar, ND; Sivasailam, B (2023). A review on welding techniques: properties, characterizations and engineering applications.

Wang, Y; Kung, L; Wang, WYC; Cegielski, CG (2018). An integrated big data analytics-enabled transformation model: Application to health care. *Informa. Manage. 55*(1): 64-79.

Wu, B; Krivtsun, I. V (2020). Processes of Nonconsumable Electrode Welding with Welding Current Modulation (Review) Part III. Modeling of the processes of TIG welding by modulated current.

Yang, T; Liu, J; Zhuang, Y; Sun, K; Chen, W (2020). Studies on the formation mechanism of incomplete fusion defects in ultra-narrow gap laser wire filling welding. *Optics & Laser Technol. 129*: 106275.

Zhang, J; Shao, P; Wang, X; Fan, D (2023). Improving weld penetration by two-TIG arc activated via mixing oxygen into shielding gas. *Inter. J. Adv. Manu. Techno. 125*(1-2): 169-181.